


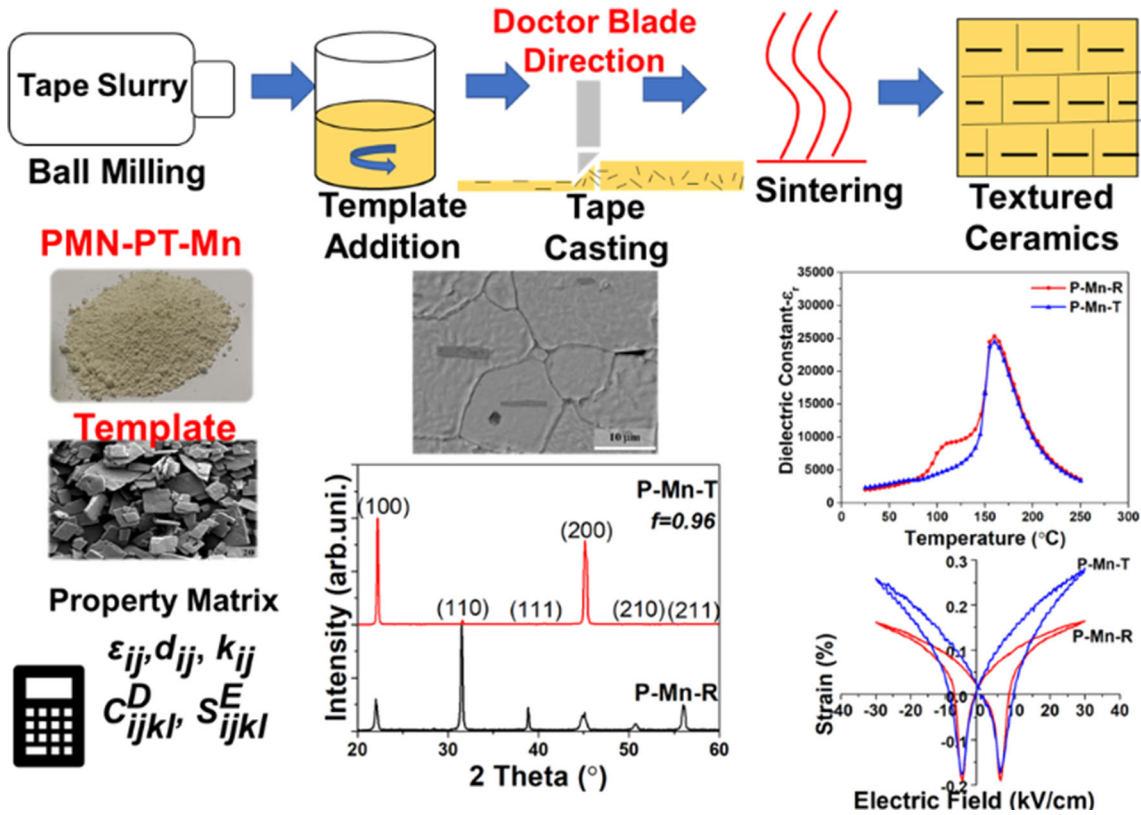
Enhanced Soft Character of Crystallographically Textured Mn-Doped Binary $0.675[\text{Pb}(\text{Mg}_{1/3}\text{Nb}_{2/3})\text{O}_3]-0.325[\text{PbTiO}_3]$ Ceramics

AYŞE BERKSOY-YAVUZ¹ and EBRU MENSUR-ALKOY ^{1,2}

1.—Department of Materials Science and Engineering, Gebze Technical University, 41400 Gebze, Kocaeli, Turkey. 2.—e-mail: ebrualkoy@gtu.edu.tr

Lead magnesium niobate (PMN)–lead titanate (PT) solid solution with composition 0.675 PMN–0.325PT has been obtained with manganese (Mn) doping in various ratios. The effect of Mn on the electrical properties was examined in detail using dry-pressed samples produced from PMN–PT powders synthesized by a solid-state calcination route. Based on the results, 0.7 mol.% was selected as the optimum Mn doping ratio to enhance the soft properties and figure of merit (FOM). Random and textured PMN–PT plates for use in energy harvesting applications were then prepared by a tape-casting method. Samples were textured using 1 vol.% plate-like barium titanate (BaTiO_3 , BT) template. The calculated FOM of random samples fabricated by tape-casting increased from $8469 \times 10^{-15} \text{ m}^2/\text{N}$ to $11,273 \times 10^{-15} \text{ m}^2/\text{N}$ with Mn doping, in parallel with observations in dry-pressed samples. The FOM of textured PMN–PT was found to be as high as $\sim 25,999 \times 10^{-15} \text{ m}^2/\text{N}$ and increased to $\sim 31,720 \times 10^{-15} \text{ m}^2/\text{N}$ for textured Mn-doped PMN–PT. The Curie temperature (T_c) of samples obtained by tape-casting was measured to be 160°C. The electromechanical properties of the samples were also studied in detail, and property matrices calculated using resonance methods are reported for all compositions.

Graphical Abstract



Key words: PMN-PT, texture, barium titanate, doping

INTRODUCTION

Studies on development of piezoelectric ceramic materials have opened up a window of possibilities for new technological applications such as micro-motors and centimeter-scale energy harvesters.¹⁻³ Lead-based ferroelectric materials are more frequently used for these applications compared with lead-free ones.⁴⁻⁸ In the case of energy harvesting applications, use of cost-effective materials with excellent properties is important for device performance. From this point of view, use of textured anisotropic materials instead of single crystals is a cost-effective method to achieve enhanced electromechanical properties compared with random polycrystalline ferroelectric materials.⁹⁻¹³

Textured ceramics with grains oriented along specific crystallographic directions can be fabricated using a combination of the templated grain growth (TGG) and tape-casting methods.¹⁰⁻¹⁵ The TGG technique consists of orientation of single-crystal template particles in a matrix, followed by high-temperature annealing that induces grain growth and densification. In recent years, there have been

an increasing number of studies¹¹⁻¹⁶ on texturing of lead-based complex perovskite solid-solution systems such as lead magnesium niobate-lead titanate [$\text{Pb}(\text{Mg}_{1/3}\text{Nb}_{2/3})\text{O}_3\text{-PbTiO}_3$] (PMN-PT) and lead indium niobate-lead magnesium niobate-lead titanate [$\text{Pb}(\text{In}_{1/2}\text{Nb}_{1/2})\text{O}_3\text{-Pb}(\text{Mg}_{1/3}\text{Nb}_{2/3})\text{O}_3\text{-PbTiO}_3$] (PIN-PMN-PT). Barium titanate (BaTiO_3 , BT) and strontium titanate (SrTiO_3 , ST) have mostly been used as template particles to texture these piezoelectric Pb-based perovskite materials.¹¹⁻¹⁴ Besides microstructural engineering, modification of the composition is another way to improve the properties of such systems. Multivalent manganese (Mn) is a doping element which is well known as a “hard” dopant that introduces oxygen vacancies that pin domain wall motion.¹⁷⁻²⁰ It was also reported²¹ that, in both single-crystal and polycrystalline ceramic systems, higher mechanical quality factor (Q_m) and coercive field (E_c) are observed when doping Mn at ratios of 1 mol.% or more.

In this study, the 0.675PMN-0.325PT binary system was investigated for use in energy harvesting applications. PMN-PT binary ceramics with

various Mn doping ratios were synthesized using a conventional solid-state calcination method. The aim of this work is to increase the piezoelectric coefficient and decrease the dielectric constant and loss to obtain a material with soft character and high figure of merit (FOM) for use in energy harvesting applications, instead of hard character for applications such as ultrasonic motors, etc. After determining the optimum Mn ratio by investigation of the electrical properties, a tape-casting method was used to produce PMN-PT plates by the TGG approach using a plate-like BT template at 1 vol.% with and without Mn addition. Finally, full property matrices, including complete sets of material constants, are also reported for the random and textured PMN-PT ceramics prepared by the tape-casting method.

EXPERIMENTAL PROCEDURES

PMN-PT ceramics were produced using two different methods: dry pressing and tape casting. Dry-pressed samples were produced with the main aim of optimizing the Mn doping ratio, whereas the tape-casting method was used to investigate the effect of texture on the PMN-PT ceramic doped with the optimum amount of Mn. However, for both fabrication methods, undoped and Mn-doped 0.675PMN-0.325PT powders were prepared using a columbite precursor method to eliminate secondary phases such as pyrochlore. In the columbite method, a precursor reaction between Nb₂O₅ (99.5%; Alfa Aesar) and 4 MgCO₃·Mg(OH)₂·5H₂O (98%; Alfa Aesar) was used to produce MgNb₂O₆. The starting reagents (PbCO₃)₂Pb(OH)₂ (Sigma Aldrich), TiO₂ (P25, rutile; Degussa), and MgNb₂O₆ (1150°C for 4 h), as well as MnO₂ (Sigma Aldrich, 99%) at varying doping ratios (0 mol.%, 0.2 mol.%, 0.4 mol.%, and 0.7 mol.%), were mixed at proper stoichiometric ratio in ethanol using ZrO₂ balls as milling medium. The powders were calcined in an alumina crucible at 750°C for 2 h. Then, 2 wt.% PbO was added to the calcined powders followed by ball-milling for 24 h to compensate for Pb loss that occurs through PbO evaporation during sintering.

For fabrication of ceramics by dry pressing, powders were dried after milling then pressed under 80 MPa into disk shape with diameter of 16 mm using binder. After sintering at 1150°C for 2 h in oxygen atmosphere, ceramic samples were ground and polished to final thickness of 1.0 mm for all samples. The sintering condition was chosen according to the results of our previous study.¹⁰ Samples prepared by dry-pressing are denoted according to their Mn content, i.e., P-0Mn, P-0.2Mn, P-0.4Mn, and P-0.7Mn.

Anisometric template particles are required to prepare crystallographically textured PMN-PT ceramics by tape casting. Plate-like anisotropic BaTiO₃ (BT) template particles were first

synthesized from Bi₄Ti₃O₁₂ (BiT) and BaBi₄Ti₄O₁₅ particles (BBT) by two-step molten salt synthesis (MSS), with a topochemical microcrystal conversation (TMC) process applied as the third stage.²² The BT template was used in the tape-casting process to prepare mainly four types of sample for comparison of their properties. First, random undoped and 0.7 mol.% Mn-doped PMN-PT samples were prepared by tape casting, denoted as P-R and P-Mn-R, respectively. Then, crystallographically textured samples were also prepared with and without 0.7 mol.% Mn using 1 vol.% BT, denoted as P-T and P-Mn-T, respectively. For preparation of the textured P-Mn-T samples, BT particles were mixed with PMN-PT slurry using a magnetic stirring bar. Then, the stable slurries were cast at rate of 10 cm/min using doctor blade height of 200 μm. The tapes were dried, cut, and laminated to prepare thicker samples. After obtaining the desired thickness, binder burnout was conducted at 600°C for 1 h, then all samples were sintered in a covered alumina crucible at 1150°C for 2 h under oxygen atmosphere. The final thickness of the samples produced by the tape-casting process were measured to be 1.0 mm for random samples and 600 μm for textured samples.

The phase content and texture fraction (*f*) of the samples were evaluated by x-ray diffraction (XRD) analysis (D8 Advance; Bruker, Germany). The texture fraction, i.e., degree of grain orientation, as measured by the Lotgering factor, was calculated from the XRD peaks of the samples in the range of 20° to 60° with Cu K_α radiation. The density of the sintered samples was measured by the Archimedes technique. The microstructure of thermally etched, fractured, and polished surfaces of the samples was observed by scanning electron microscopy (SEM, Philips XL30, FEI Co., USA). For electrical measurements, both sides of the samples were polished to obtain parallel surfaces, and silver paste was applied to the surfaces of the sintered sample parallel to the tape-casting direction. The electrodes were fired at 600°C for 30 min. Polarization-electric field (*P-E*) loops were measured using a Precision LC ferroelectric tester (Radiant Technologies, Inc., USA), and the electric-field-induced strain was determined using an MTI 2000 photonic sensor (MTI Instrument Inc., USA) at room temperature. Samples immersed in silicone oil were poled at 80°C under a direct-current electric field of 30 kV/cm for 15 min, then aged for 24 h before measurements. The dielectric constant (ϵ_r) and dielectric loss ($\tan \delta$) as functions of temperature were taken at 10 kHz using a multifrequency inductance-capacitance-resistance meter (LCR, Hioki, Japan) in the temperature range of 25°C to 250°C at 2°C/min. The piezoelectric charge coefficient (d_{33}) was measured directly using a piezo- d_{33} meter (APC International Ltd., USA). Full matrices of material constants were evaluated according to IEEE standards using the resonance method.

RESULTS AND DISCUSSION

Effect of Mn Doping on Structural and Electrical Properties of PMN-PT

Lead magnesium niobate–lead titanate (PMN-PT) powders were first synthesized by a solid-state calcination method following the columbite precursor route without and with Mn doping at ratios of 0.2 mol.%, 0.4 mol.%, and 0.7 mol.%; these samples are denoted as P-*x*Mn (*x* = 0.0, 0.2, 0.4, and 0.7). XRD analysis revealed that all samples crystallized in perovskite phase without presence of secondary phases (Fig. 1). According to cross-sectional SEM, all samples were dense.

The temperature dependence of the dielectric constant (ϵ_r) and dielectric loss ($\tan \delta$) of the poled samples was also investigated for the samples with various Mn doping ratios (Fig. 2a and b). The first phase transition was observed at $\sim 110^\circ\text{C}$ to 115°C for undoped and Mn-doped samples (Fig. 2a). In literature, this phase transition is reported to be from ferroelectric (FE) rhombohedral to FE tetragonal phase. It is also reported that rhombohedral structure is obtained at room temperature for the PMN-PT binary system.^{13,15–17} It is also seen from Fig. 2a that the tetragonal FE to cubic paraelectric phase transition temperature, i.e., the Curie temperature (T_c), was $\sim 170^\circ\text{C}$ for the undoped (P-0Mn) and 0.2% Mn-doped (P-0.2Mn) samples. However, when the Mn ratio was increased to 0.4% or 0.7%, the T_c value decreased slightly to $\sim 165^\circ\text{C}$ (Fig. 2a). The peak value of the dielectric constant at the transition temperature increased drastically for initial Mn doping of 0.2 mol.%. This is due to Mn acting either as a donor dopant at the Mg^{2+} site or as an isovalent substituent with smaller size at the Ti^{4+} site. It is believed that a mixture of both occurs, due to the multivalent nature of the Mn cation, as

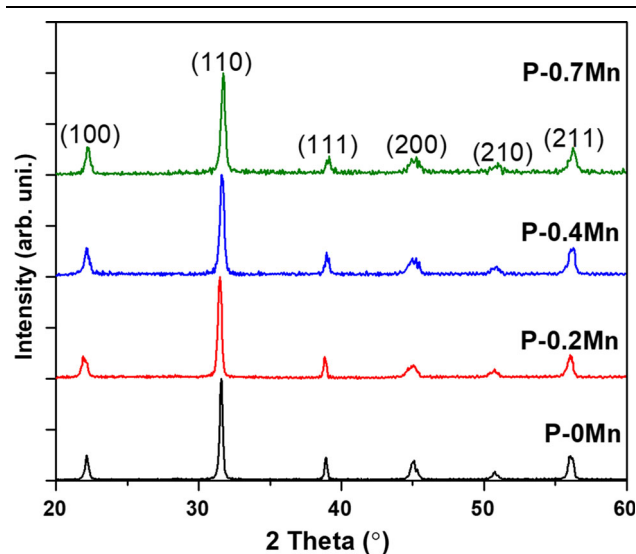


Fig. 1. Indexed XRD pattern of undoped and Mn-doped PMN-PT samples produced by dry-pressing method.

discussed below. Further increase in the Mn content led to a decrease in the peak value of the dielectric constant, although it remained higher than for the undoped case. The dielectric loss of undoped and Mn-doped PMN-PT also displayed similar behavior, with $\tan \delta$ initially increasing with 0.2 mol.% Mn doping then decreasing with further increase in the Mn content (Fig. 2b).

The electric field-induced polarization and bipolar strain behavior of all samples were measured under a field of 30 kV/cm. A consistent increase in the remanent polarization with increasing Mn content was observed (not shown here). The strain versus electric field data presented in Fig. 3, on the other hand, indicate an initial increase in the strain levels of PMN-PT with 0.2 mol.% Mn doping, followed by a slight decrease at higher doping ratios. However, the maximum strain levels at the highest drive fields were still higher than for the undoped case, indicating the positive effect of Mn doping on the electromechanical properties. All measured data

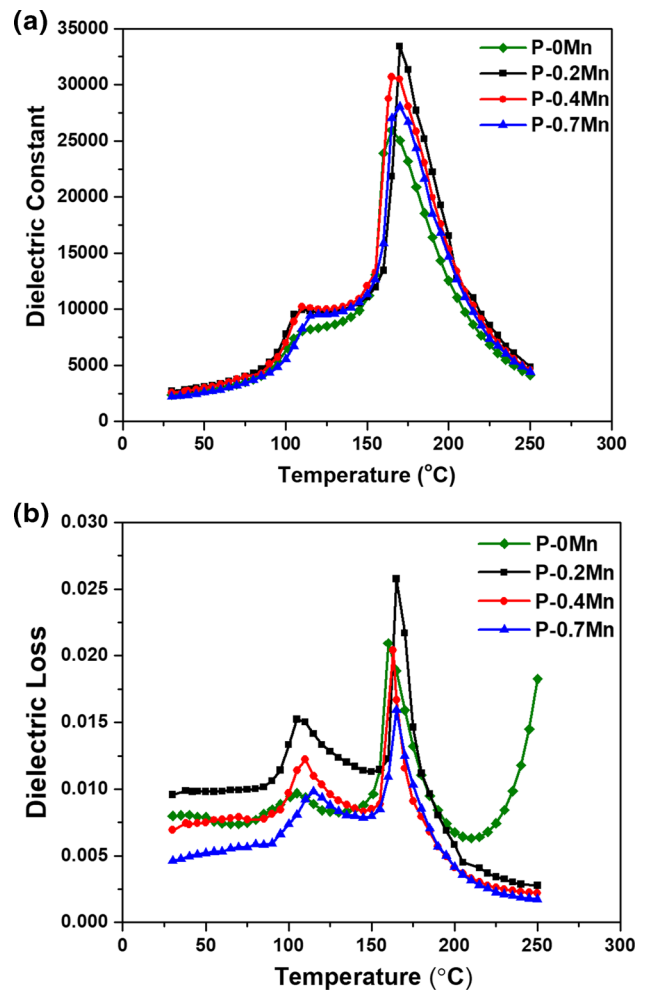


Fig. 2. Variation of (a) dielectric constant and (b) tangent loss with temperature of undoped and Mn-doped PMN-PT samples produced by dry-pressing method.

such as the remanent polarization (P_r), coercive field (E_c), piezoelectric charge coefficient (d_{33}), dielectric constant (ϵ_r), and dielectric loss ($\tan \delta$), along with calculated data such as the mechanical quality factor (Q_m), electromechanical coupling coefficient (k_p), and piezoelectric voltage coefficient (g_{33}), are presented in Table I, revealing that d_{33} increased consistently with increasing Mn ratio then decreased abruptly at 0.7 mol.%, thus higher Mn ratios were not investigated in this study. A figure of merit (FOM) for energy harvesting applications was also calculated for each composition and is given in Table I. The FOM depends on the piezoelectric charge and voltage coefficients, i.e., $d_{33} \times g_{33}$, where the piezoelectric voltage coefficient, g_{33} , is in turn directly proportional to d_{33} and inversely proportional to the dielectric constant.²³ Energy harvesting applications also require low dielectric loss. The decrease in ϵ_r was more drastic at higher Mn ratios, leading to the highest FOM for the 0.7 mol.% Mn-doped sample (P-0.7Mn), whereas $\tan \delta$ was lowest in the case of 0.7 mol.% Mn doping.

As seen from the data discussed above and given in Table I and figures, it is clear that Mn had a positive effect on the electrically soft character of the PMN-PT ceramic, whereas it is known from

literature that Mn is usually added to perovskite piezoelectrics to provide hard character. It is reported in literature by Park et al.¹⁹ that, while Q_m remained almost constant or changed slightly upon 0.5 mol.% Mn addition, it increased fivefold with 1 mol.% Mn addition. Meanwhile, 2 mol.% Mn doping increased Q_m almost ninefold compared with pure PMN-PZT, while the d_{33} coefficient was found to decrease with Mn addition at this ratio.²⁰ Thus, the effect of Mn doping requires more thorough discussion to explain the current results.

Manganese is a multivalent cation and is usually referred to in literature as a B-site acceptor dopant in the ABO₃ structure, with 2+ or 3+ oxidation state. Acceptor dopants are expected to induce electrically hard character, essentially leading to a decrease in the dielectric, piezoelectric, and ferroelectric properties. However, Mn can actually assume oxidation states varying from 2+ to 7+.²⁴ In our study, Mn was added as MnO₂, i.e., in the form of Mn⁴⁺. Additionally the B-site position in the PMN-PT perovskite lattice is actually occupied by three different cations with different oxidation states. The particular composition investigated in our study, viz. 0.675[Pb(Mg_{1/3}Nb_{2/3})O₃]-0.325[PbTiO₃], indicates that, of all the available B-sites that the Mn dopant could occupy, 32.5% are filled with Ti⁴⁺, 45% with Nb⁵⁺, and 22.5% with Mg²⁺. Thus, the B-site cation that Mn replaces and the oxidation state of Mn itself will determine whether it will act as an acceptor or an isovalent or donor dopant.

In our study, Mn addition at up to 0.7 mol.% enhanced the soft character of the ceramic. We therefore conclude that, when small amounts of Mn are added to PMN-PT, Mn assumes 2+, 3+, or 4+ oxidation state. In that case, it either replaces Mg²⁺ as an isovalent or donor dopant, or Mn⁴⁺ replaces Ti⁴⁺, acting as an isovalent dopant. Donor doping is known to enhance the piezoelectric and ferroelectric properties through increased domain wall motion. In the case of an isovalent dopant, Mn²⁺ is smaller than Mg²⁺ and Mn⁴⁺ is smaller than Ti⁴⁺.²⁴ Replacing a larger B-site cation with a smaller one in the perovskite lattice would provide a larger space for the smaller ion to displace under alternating electric fields, leading to enhanced polarization, according to Uchino's rattling-ion model.²⁵ The oxidation state in the 0.7 mol.% Mn-doped PMN-PT sample was investigated by x-ray

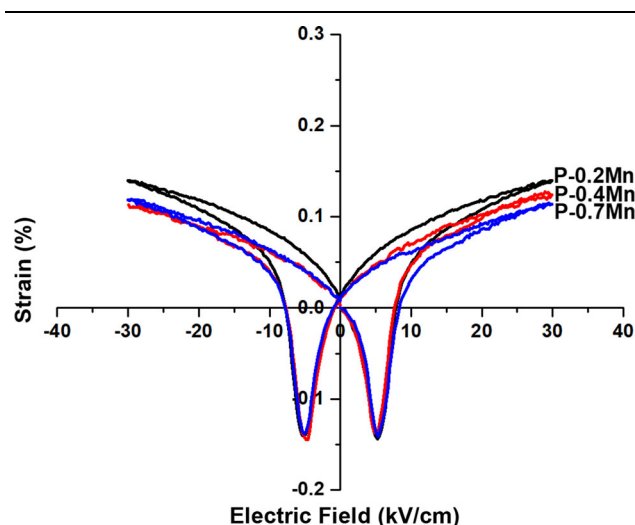


Fig. 3. Comparison of electric field-induced bipolar strain curves of Mn-doped PMN-PT samples produced by dry-pressing method.

Table I. Electrical properties of PMN-PT samples prepared by dry pressing

Sample	d_{33}^*		P_r		S (%) at		Q_m	k_p	g_{33}	$d_{33} \times g_{33}$
MnO ₂ (mol.%)	d_{33} (pC/N)	(pm/V) at 30 kV/cm	ϵ_r	$\tan \delta$ (%)	($\mu\text{C}/\text{cm}^2$) at 30 kV/cm	30 kV/cm				
0	400	363	2380	0.79	28	0.10	113	0.58	18.98	7592
0.2	465	438	2700	0.96	32	0.14	98	0.68	19.45	9044
0.4	480	397	2568	0.69	33	0.13	96	0.69	21.11	10,132
0.7	450	383	2233	0.44	33	0.12	137	0.68	22.76	10,242

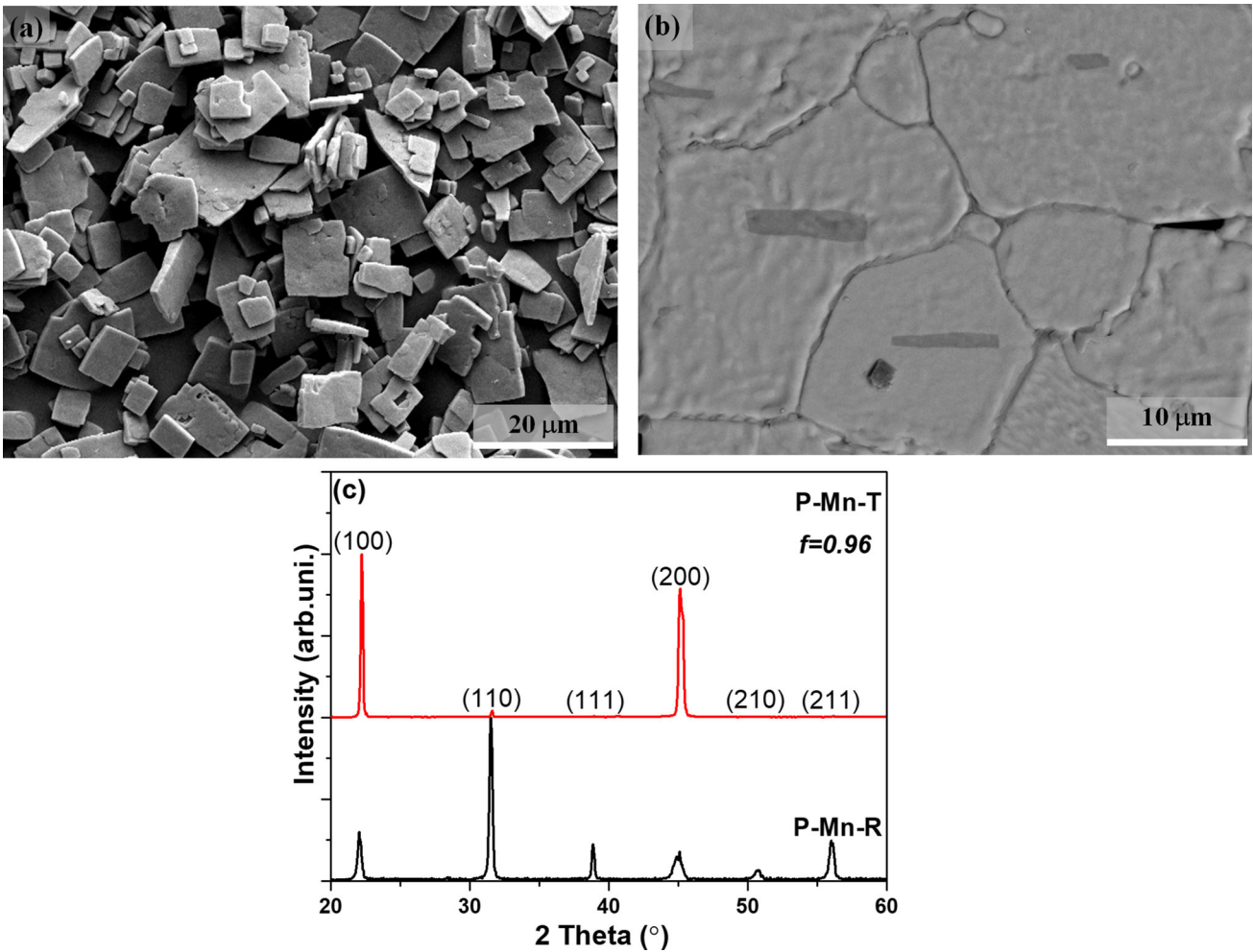


Fig. 4. SEM micrographs of (a) BT template and (b) cross-section of 0.7 Mn-doped PMN–PT textured with 1 vol.% BT template (P-Mn-T); (c) indexed XRD patterns of P-Mn-R and P-Mn-T samples.

photoelectron spectroscopy (XPS) analysis to resolve this issue. However, when the XPS spectra of the sample were investigated in detail (not presented here), it was determined that, of the three peaks identifying Mn that could be used to resolve the oxidation state of manganese, that for Mn $2p^{3/2}$ overlapped with that for Pb $4p^{3/2}$ at ~ 645 eV, that for Mn $3s$ overlapped with that for Pb $5p^{3/2}$ at ~ 83 eV, and that for Mn $3p$ overlapped with that for Mg $2p$ at ~ 48 eV. Additionally, since the Mn content in the ceramic was limited to 0.7 mol.%, the signal from the Mn was rather weak. Thus, it was not possible to identify the Mn oxidation state by XPS analysis.

Since the final aim of this study is to optimize the electrical and electromechanical properties of PMN–PT thin ceramic plates for use in energy harvesting applications, ceramics with electrically soft character are desired. According to the results in Table I, PMN–PT with 0.7 mol.% Mn addition

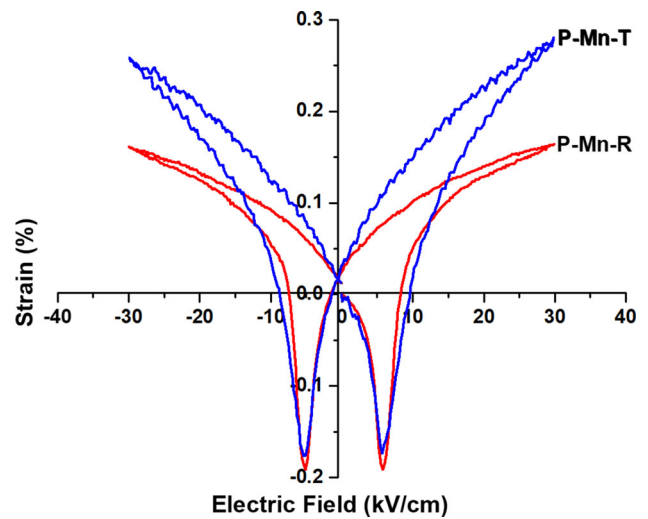


Fig. 5. Comparison of electric field-induced bipolar strain curves of P-Mn-R and P-Mn-T samples.

Table II. Electrical properties of PMN-PT samples produced by tape-casting

Sample	d_{33} (pC/N)	d_{33}^* (pm/V)	ϵ_r	$\tan \delta$ (%)	P_r ($\mu\text{C}/\text{cm}^2$)	S (%)	Q_m	k_p	$(\times 10^{-3} \text{ V m/N})$	$d_{33} \times g_{33}$ ($\times 10^{-15} \text{ N/m}^2$)
P-R	405	364	2188	0.68	29	0.11	63	0.65	20.91	8469
P-T	690	865	2068	0.56	25	0.26	144	0.81	37.68	25,999
P-Mn-R	455	373	2029	0.27	34	0.12	143	0.66	25.33	11,525
P-Mn-T	810	887	2336	1.94	29	0.27	175	0.85	39.16	31,720

seemed to be the optimum composition to obtain the highest FOM of $10,242 \times 10^{-15} \text{ m}^2/\text{N}$, while the undoped PMN-PT ceramic showed FOM of $7592 \times 10^{-15} \text{ m}^2/\text{N}$. However, this FOM value for the 0.7 mol.% Mn-containing PMN-PT must still be increased further for better energy harvesting performance. The next section discusses the results of our further efforts towards this aim.

Effect of Crystallographic Texture and Doping on Structural and Electrical Properties of PMN-PT

Development of crystallographic texture is another way to enhance the properties along certain crystallographic directions. The properties of undoped and 0.7 mol.% Mn-doped PMN-PT samples with and without texture prepared by the tape-casting process are reported in this section. Tape-casting not only provides textured microstructure but also allows fabrication of thinner ceramic plates that are suitable for use in energy harvesting applications. A templated grain growth process was used to obtain textured ceramics, using plate-like barium titanate (BT) single-crystal particles, synthesized by a topochemical microcrystal conversion method,²² as the template. The mean size and lateral dimensions of the template particles were calculated to be $\sim 6 \mu\text{m} \times 6 \mu\text{m} \times 0.7 \mu\text{m}$ (length \times width \times thickness) on average. SEM examination revealed that the width and thickness of the platelets were rather uniform, and although the average length was $6 \mu\text{m}$, there were platelets with length of up to $12 \mu\text{m}$ (Fig. 4a). Detailed experimental results for the BT template ratio and its influence on the electrical properties of PMN-PT are also reported in literature.^{13,21} In this study, in light of reported results and our previous study,¹⁰ samples were fabricated with 1.0 vol.% BT addition by tape-casting.

A cross-sectional SEM micrograph of the textured Mn-doped sample (P-Mn-T) is shown in Fig. 4b. The BT template is clearly seen in this figure, embedded in the center of the grain with darker contrast. The template particles were found to be highly aligned along the tape-casting direction, as expected. The XRD patterns of the randomly oriented and textured Mn-doped PMN-PT samples (P-Mn-R and P-Mn-T, respectively) are shown in Fig. 4c, clearly revealing that use of the BT template and

application of the appropriate heat treatment necessary for the templated grain growth process induced (001) texture in the ceramics with degree of grain orientation, as measured by the Lotgering factor,²⁶ f , calculated to be 0.96. The Lotgering factor of the textured sample without Mn doping, i.e., the P-T sample, was calculated as 0.90 (not shown in the figure).

Electric field-induced polarization, and unipolar and bipolar strain measurements were carried out at electric field up to 30 kV/cm. The electric field-induced strain behavior of the P-Mn-R and P-Mn-T samples is shown in Fig. 5. The results of all the dielectric, ferroelectric, and piezoelectric measurements are presented in Table II. Texturing of the ceramic increased the electromechanical properties, as seen in Fig. 5 and Table II. It can be seen from Fig. 5 that the (001)-textured ceramic showed high strain with maximum of $\sim 0.30\%$ at field of 30 kV/cm, twice that ($\sim 0.15\%$) observed for the random sample with the same composition. While the high-field piezoelectric coefficient (d_{33}^*) of the P-Mn-R sample determined from the slope of the strain curves in the high-field region (30 kV/cm) was 373 pC/N, this value was measured as 887 pC/N for the textured P-Mn-T sample (Table II).

The piezoelectric charge coefficient (d_{33}) is one of the important parameters to enhance the soft character and FOM for specific applications. The results in Table II already show that Mn doping increased the d_{33} coefficient. According to Table II and Fig. 5, the d_{33} value of textured PMN-PT was increased from 690 pC/N to 810 pC/N with Mn doping. The dielectric loss was found to be 0.4% in both cases, indicating that its effect on the FOM would be at the same level for both of the textured samples. In summary, the FOM value calculated for the P-R sample fabricated by tape-casting was increased from $8469 \times 10^{-15} \text{ m}^2/\text{N}$ to $11,525 \times 10^{-15} \text{ m}^2/\text{N}$ with Mn doping, in parallel with the observations on dry-pressed samples in the first part of this study. However, the FOM value of the textured PMN-PT (sample P-T), was found to be as high as $\sim 25,999 \times 10^{-15} \text{ m}^2/\text{N}$. For textured Mn-doped PMN-PT (P-Mn-T sample), this value was calculated to be $\sim 31,720 \times 10^{-15} \text{ m}^2/\text{N}$, proving the drastic effect of combining Mn doping and crystallographic texture. As a result, the FOM increased almost threefold with texturing, clearly indicating that microstructural and domain

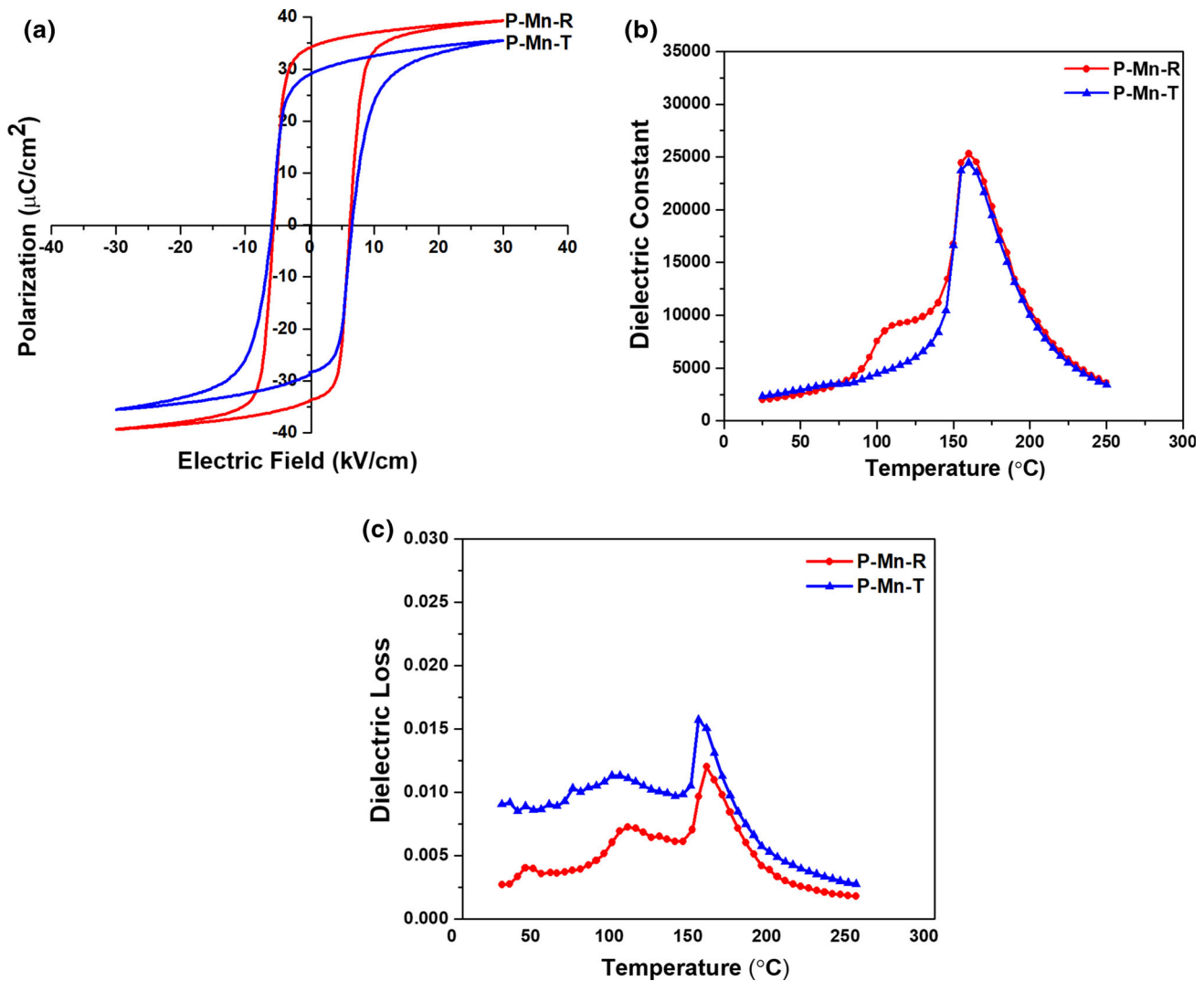


Fig. 6. Comparison of (a) electric field-induced polarization, (b) dielectric constant, and (c) tangent loss with temperature for P-Mn-R and P-Mn-T samples.

engineering had the greatest effect on the properties. However, it is also clear that Mn addition provided an unquestionable contribution to the properties. The FOM obtained in this study was also compared to values calculated from literature; For example, Yan et al.²⁰ reported that the highest values of d_{33} and g_{33} for nontextured undoped 0.675PMN–0.325PT were ~ 475 pC/N and $\sim 17.7 \times 10^{-3}$ V m/N, respectively. The FOM value calculated for that sample was higher than that of the P-R sample in this study, which can be attributed to differences in processing conditions and chemical sources. However, with texturing, Yan et al.²⁰ reported that the highest value of d_{33} and g_{33} of undoped 0.675PMN–0.325PT textured with BT increased to ~ 650 pC/N and $\sim 27 \times 10^{-3}$ V m/N, respectively. These values corresponds to a FOM that is 33% lower than that for the textured undoped P-T sample in this study. Poterala et al.¹³ also reported that the d_{33} and g_{33} values of undoped

0.675 PMN–0.325PT textured using sodium bismuth titanate–lead titanate template particles were ~ 855 pC/N and $\sim 27.7 \times 10^{-3}$ V m/N, respectively. The FOM value calculated for that study is $\sim 23,940 \times 10^{-15}$ m²/N, comparable to but lower than the FOM of the P-T sample in this work. Poterala et al.¹³ also reported that the FOM of a textured sample decreased with 2% Mn addition, whereas in our study, 0.7% Mn addition provided a 22% increment in the FOM. Thus, the remarkable contribution of this study is the effect of a controlled amount of Mn doping on the soft properties and FOM of the textured ceramic, with content of 0.7% being found to be optimum after detailed investigation.

The electric field-induced polarization hysteresis measurements on random and textured ceramics with and without Mn doping indicated that the remanent polarization decreased with texturing in both cases (Fig. 6a). This is against expectations,

Table III. Full properties of PMN-PT samples prepared according to the IEEE standards

Property	Undoped		0.7 mol.% Mn Doping		PZT-5A ^a
	Random (P-R)	Textured (P-T)	Random (P-Mn-R)	Textured (P-Mn-T)	
P (kg/m ³)	8060	8020	8170	8050	7600
k_p	0.65	0.81	0.66	0.85	0.62
k_t	0.48	0.61	0.54	0.60	0.50
k_{31}	0.38	0.45	0.42	0.47	0.35
k_{33}	0.75	0.89	0.78	0.91	0.73
k_{15}	0.50	0.54	0.49	0.44	0.58
d_{31} (pC/N)	-160	-217	-178	-255	-275
d_{15} (pC/N)	371	370	283	311	451
d_{33} (pC/N)	400	690	455	816	435
S_{11}^E ($\times 10^{-12}$ m ² /N)	10.4	15.1	10.2	14.0	14.9
S_{12}^E ($\times 10^{-12}$ m ² /N)	-3.4	-5.9	-2.9	-5.4	-3.2
S_{13}^E ($\times 10^{-12}$ m ² /N)	-5.6	-11.4	-5.5	-10.3	-11
S_{33}^E ($\times 10^{-12}$ m ² /N)	16.5	39.3	16.7	38.3	29.7
S_{44}^E ($\times 10^{-12}$ m ² /N)	30.2	31.8	27.4	25.4	38.7
S_{66}^E ($\times 10^{-12}$ m ² /N)	27.4	41.9	26.4	38.9	34.3
$\varepsilon_{11}^T/\varepsilon_0$	2764	2373	2084	2448	2645
$\varepsilon_{33}^T/\varepsilon_0$ (1 kHz)	2248	1866	2015	2413	2203
$\varepsilon_{33}^T/\varepsilon_0$ (10 kHz)	2188	2072	2029	2336	2150
Q_m	63	144	143	175	59
$\tan \delta$ (%) (10 kHz)	0.7	0.6	0.3	0.9	2.7

^aPressed sample produced from commercially available PZT-5A powder from Sunny-Tech Company (Taiwan).

since texture development is usually expected to enhance the properties in general. Closer investigation is required to explain this decrease in the remanent polarization. Thus, the temperature dependence of the dielectric constant and dielectric loss of the textured samples prepared by tape casting was measured and is shown in Fig. 6b and c. From this figure, it is observed that the first phase transition peak (T_{M-T}) of the textured sample P-Mn-T disappeared, whereas it was clearly present for the random sample. The T_c value for both samples was measured to be 160°C. The peak maximum levels of ε_r were almost the same for both P-Mn-R and P-Mn-T samples. These temperature-dependent values and behaviors are in good agreement with literature.¹⁵

The disappearance of the rhombohedral to tetragonal phase transition may indicate that the tetragonal structure is stabilized down to room temperature in the textured ceramic, probably due to elastic boundary conditions created on the unit cells and grains by the crystallographic texture itself. Another explanation would be suppression of the rhombohedral to tetragonal phase transition by the clamping effect of the BT template, because of the slightly changing slope in the phase-transition region.^{10,11,15} The stresses arising from this effect may stabilize one FE phase while suppressing the transition to the other. The polarization directions

in the rhombohedral phase are along the $[111]_{pc}$ direction.²⁷ However, their orientation should induce higher polarization along the $[001]_{pc}$ direction in $[001]_{pc}$ -cut single crystals, or in $[001]_{pc}$ -textured ceramics and thin films, through the combination of multiple domains, i.e., domain engineering.¹⁷ Meanwhile, the polarization in the tetragonal phase is along the $[001]_{pc}$ direction, and single crystals cut along $[001]_{pc}$ or ceramics and thin films textured along $[001]_{pc}$ would be expected to show lower properties compared with the rhombohedral phase, due to the limited number of favorably oriented domains. As a result, disappearance of the rhombohedral to tetragonal phase transition and stabilization of the tetragonal phase down to room temperatures would lead to lower remanent polarization in the hysteresis behavior.

The full electromechanical properties of the random and textured undoped and Mn-doped samples were measured and calculated using the resonance method. The dimensions of the samples were suitable for recommended IEEE standards for the resonance method.^{28,29} The admittance and phase angle of the samples were measured as functions of frequency. The electromechanical properties of textured PMN-PT were calculated, assuming ∞ m Curie group symmetry for a poled ferroelectric ceramic, as reported in literature.^{15,30} The complete sets of properties for the textured and random

undoped and Mn-doped PMN–PT samples are presented in Table III, in comparison with commercially available soft piezoelectric ceramic (PZT-5A). The data for the elastic compliance coefficients (s_{ij}^E), electromechanical coupling coefficients (k_{ij}), piezoelectric coefficients (d_{ij}), and dielectric permittivities (ϵ_{ij}^T) of all samples are presented in Table III. The relative permittivity values ϵ_{11} and ϵ_{33} of the textured samples reveal that undoped and doped PMN–PT were almost dielectrically isotropic. Addition of 0.7 mol.% Mn did not affect the dielectric permittivity. The electromechanical properties displayed drastic increases with Mn doping and texture development. The compliance coefficients along the poling axis, s_{33} , of both undoped and doped samples were increased by texturing. While the s_{33} value of the random PMN–PT sample was $16.5 \times 10^{-12} \text{ m}^2/\text{N}$, it reached $39.3 \times 10^{-12} \text{ m}^2/\text{N}$ with texturing. The samples with Mn doping exhibited comparable values of s_{33} (Table III). All data are in agreement with literature.¹⁵

CONCLUSIONS

Undoped and 0.2 mol.%, 0.4 mol.%, and 0.7 mol.% Mn-doped PMN–PT samples were fabricated using a dry-pressing method. The FOM for energy harvesting applications depends on the piezoelectric charge and voltage coefficients, i.e., $d_{33} \times g_{33}$, where the piezoelectric voltage coefficient, g_{33} , is in turn directly proportional to d_{33} and inversely proportional to the dielectric constant. While the FOM for undoped PMN–PT was calculated to be $7592 \times 10^{-15} \text{ m}^2/\text{N}$, it reached its highest value of $10,242 \times 10^{-15} \text{ m}^2/\text{N}$ for the 0.7 mol.% Mn-doped PMN–PT sample. The aim of this study was enhancement of the soft character; since especially d_{33} decreased drastically after 0.7 mol.% Mn doping, resulting in poor FOM values, Mn doping beyond this limit was not investigated and this composition was chosen as the optimum for further study.

The next step for energy harvesting applications was to produce ceramics in thin plate form with enhanced electrical properties. Random ceramic plates without and with 0.7 mol.% Mn doping were produced using a tape-casting method. Crystallographically textured ceramics were also fabricated using 1 vol.% BT template in the PMN–PT structure to improve the electrical properties. After detailed investigation, the FOM reached $\sim 31,720 \times 10^{-15} \text{ m}^2/\text{N}$ for the textured Mn-doped PMN–PT sample, representing an almost fivefold increase compared with the random undoped ceramic produced by dry pressing. Another contribution of this study is that full property matrices for the random and textured samples were measured, calculated, and reported using resonance methods, according to IEEE standards. Drastic increases

were observed in the electromechanical properties of the textured Mn-doped ceramic.

ACKNOWLEDGEMENTS

The authors wish to acknowledge financial support from the Turkish Academy of Sciences and TUBITAK project #217M086.

REFERENCES

1. M. Umeda, K. Nakamura, and S. Ucha, *J. Appl. Phys.* 35, 3267 (1996).
2. J. Lim, C. Park, J. Kim, S. Jeong, M. Kim, and T. Park, *J. Electroceram.* 30, 108 (2013).
3. J. Lim, S. Jeong, N. Kim, S. Cheon, M. Kim, and T. Park, *Ceram. Int.* 39, 641 (2013).
4. E. Mensur-Alkoy, A. Berksoy-Yavuz, and S. Alkoy, *J. Am. Ceram. Soc.* 97, 3425 (2014).
5. E. Mensur-Alkoy and A. Berksoy-Yavuz, *Bol. Soc. Esp. Ceram. Vidrio* 55, 246 (2016).
6. E. Mensur-Alkoy and A. Berksoy-Yavuz, *IEEE Trans. Ultrason. Ferroelec. Freq. Cont.* 59, 2121 (2012).
7. E. Mensur Alkoy, *J. Appl. Phys.* 108, 094104 (2010).
8. E. Mensur Alkoy and M. Papila, *Ceram. Int.* 36, 1921 (2010).
9. Y. Saito, H. Takao, T. Tani, T. Nonoyama, K. Takatori, T. Homma, T. Nagaya, and M. Nakamura, *Nature* 432, 84 (2004).
10. A. Berksoy-Yavuz and E. Mensur-Alkoy, *J. Mater. Sci. Mater. Electron.* Accepted (2018). <https://doi.org/10.1007/s10854-018-9455-8>.
11. Y. Yan, Y.U. Wang, and S. Priya, *Appl. Phys. Lett.* 100, 192905 (2012).
12. Y. Yan, L. Yang, Y. Zhou, K. Cho, J.S. Heo, and S. Priya, *J. Appl. Phys.* 118, 104101 (2015).
13. S.F. Poterala, S. Trolier-McKinstry, R.J. Meyer, and G.L. Messing, *J. Appl. Phys.* 110, 014105 (2011).
14. S. Kwon, E.M. Sabolsky, G.L. Messing, and S. Trolier-McKinstry, *J. Am. Ceram. Soc.* 88, 312 (2005).
15. E.M. Sabolsky, A.R. James, S. Kwon, S. Trolier-McKinstry, and G.L. Messing, *Appl. Phys. Lett.* 78, 2551 (2001).
16. Y. Chang, Y. Sun, J. Wu, X. Wang, S. Zhang, B. Yang, G.L. Messing, and W. Cao, *J. Eur. Ceram. Soc.* 36, 1973–1981 (2016).
17. S.-E. Park and T.R. Shrout, *J. Appl. Phys.* 82, 1804 (1997).
18. X. Qi, E. Sun, J. Wang, R. Zhang, B. Yang, and W. Cao, *Ceram. Int.* 42, 15332 (2016).
19. J.H. Park, J. Park, J.G. Park, B.K. Kim, and Y. Kim, *J. Eur. Ceram. Soc.* 21, 1383 (2001).
20. Y. Yan, K.-H. Cho, and S. Priya, *J. Am. Ceram. Soc.* 94, 1784–1793 (2011).
21. Y. Yan, K.H. Cho, and S. Priya, *J. Am. Ceram. Soc.* 100, 132908 (2012).
22. D. Liu, Y. Yan, and H. Zhou, *J. Am. Ceram. Soc.* 90, 1323 (2007).
23. R.A. Islam and S. Priya, *Appl. Phys. Lett.* 88, (2006).
24. R.D. Shannon, *Acta Cryst.* A32, 751–767 (1976).
25. K. Uchino, L.E. Cross, R.E. Newnham, and S. Nomura, *Phase Transit.* 1, 333 (1980).
26. S.L. Swartz and T.R. Shrout, *Mater. Res. Bull.* 17, 1245 (1982).
27. E.B. Araújo, *Advances in Ceramics—Electric and Magnetic Ceramics, Bioceramics, Ceramics and Environment* (Den Haag: IntechOpen, 2011), p. 50.
28. IEEE Standard on Piezoelectricity, ANSI/IEEE Std. 176-1987 (1988) <https://doi.org/10.1109/ieeestd.1988.79638>.
29. M. Algueró, C. Alemany, L. Pardo, and A.M. Gonzalez, *J. Am. Ceram. Soc.* 87, 209 (2004).
30. S. Zhang, E.F. Alberta, R.E. Eitel, C.A. Randall, and T.R. Shrout, *IEEE Trans. Ultrason. Ferroelec. Freq. Cont.* 52, 2131 (2005).